Electronic Supplementary Material (ESI) for Lab on a Chip.

Electronic Supplementary Information

Understanding droplet breakup in a post-array device with sheath-flow configuration

Shuzo Masui, Yusuke Kanno, Takasi Nisisako*

Institute of Innovative Research, Tokyo Institute of Technology, Yokohama, Kanagawa, Japan

***To whom correspondence should be addressed:**

E-mail: nisisako.t.aa@m.titech.ac.jp

Tel/fax: +81-45-924-5092

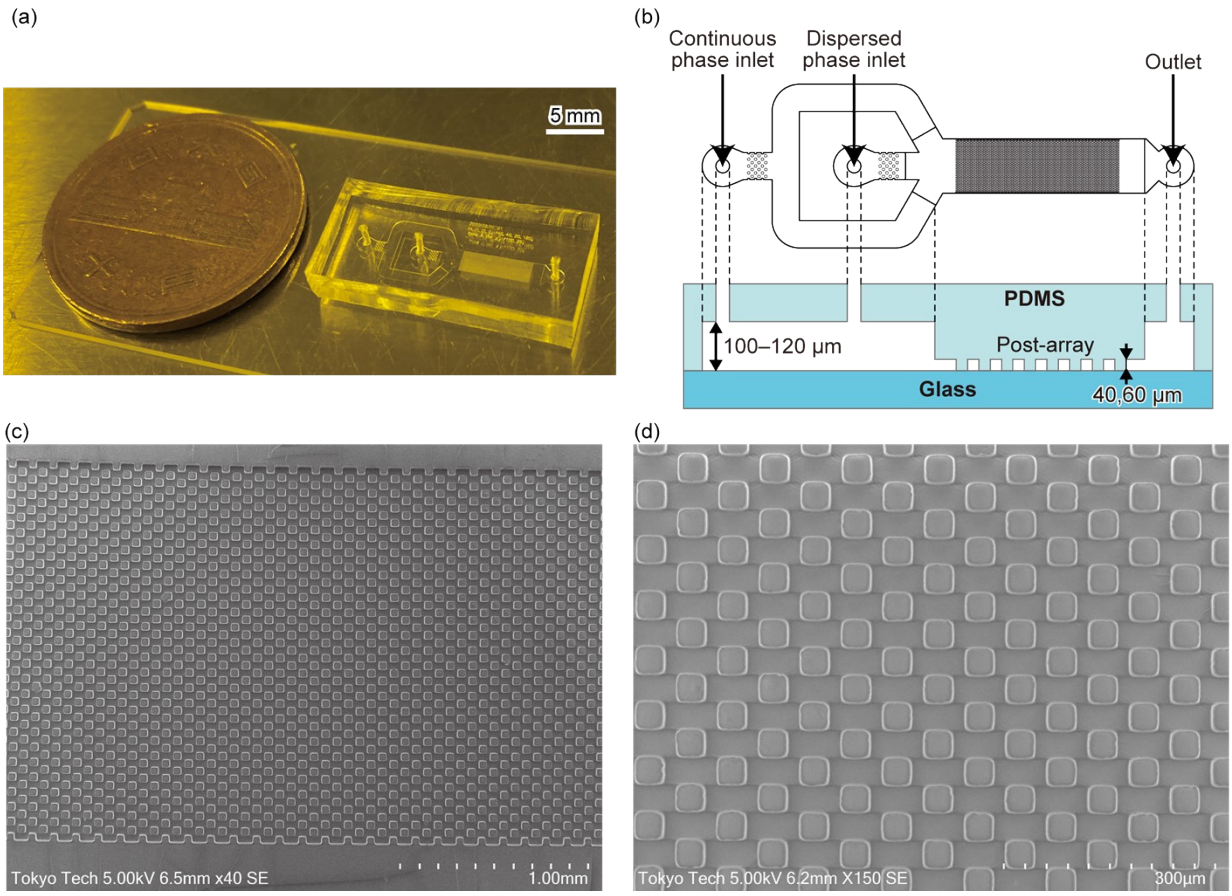

Figure S1 - (a) Photograph, (b) schematic illustration of the PDMS post-array device, and (c, d) scanning electron microscope images of post array in "Standard" device #1.

Swelling test of a surface-treated PDMS chip for hexadecane and liquid paraffin

First, a PDMS device in which hydrophilic surface treatment was conducted as described in the experimental section was filled with hexadecane or liquid paraffin. The increase in post width over time was measured by image processing. As a result, The increase in the post area almost saturated as 2.8% after 10 minutes of hexadecane immersion, or 1.7% in linear expansion ratio. Furthermore, in the O/W droplet generation, hexadecane was used as the dispersed phase, so the swelling effect was considered even smaller. Therefore, in our study, the swelling of PDMS due to hexadecane was ignored.

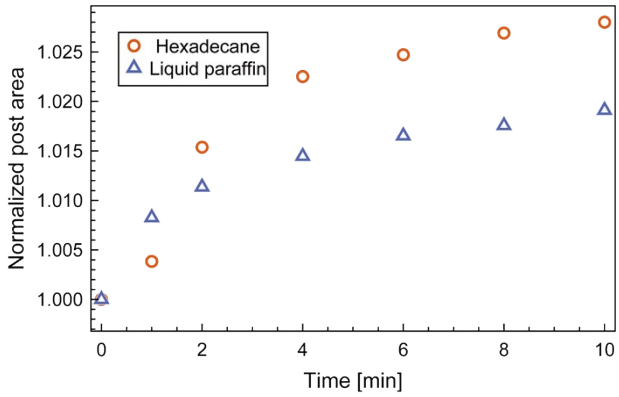

Figure S2 Variation normalized post area by swelling of the surface treated PDMS post-array chip in hexadecane and liquid paraffin.

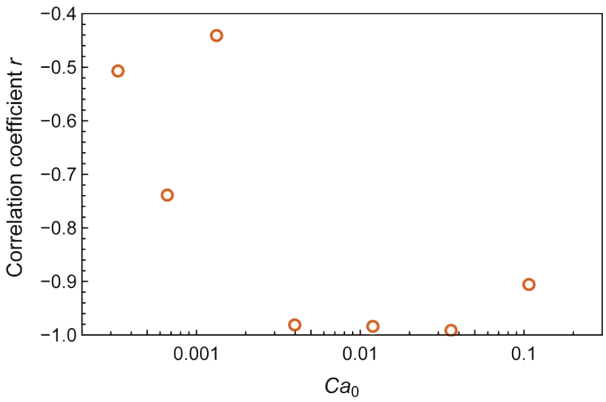

Figure S3 - Plot of correlation coefficient r between fraction φ and mean droplet diameter D_{mean} for Ca_0 = 0.0002–0.012. The presented data was calculated from the same data as Fig. 3 in the main text.

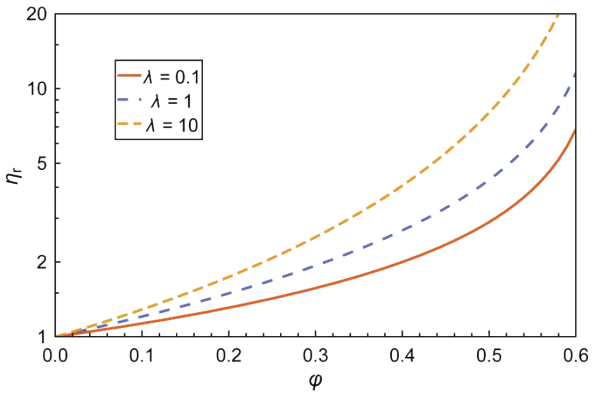

Figure S4 - Relationship between dispersed phase fraction φ and relative viscosity of emulsion η_r calculated for three viscosity ratios: λ = 0.1, 1, and 10.

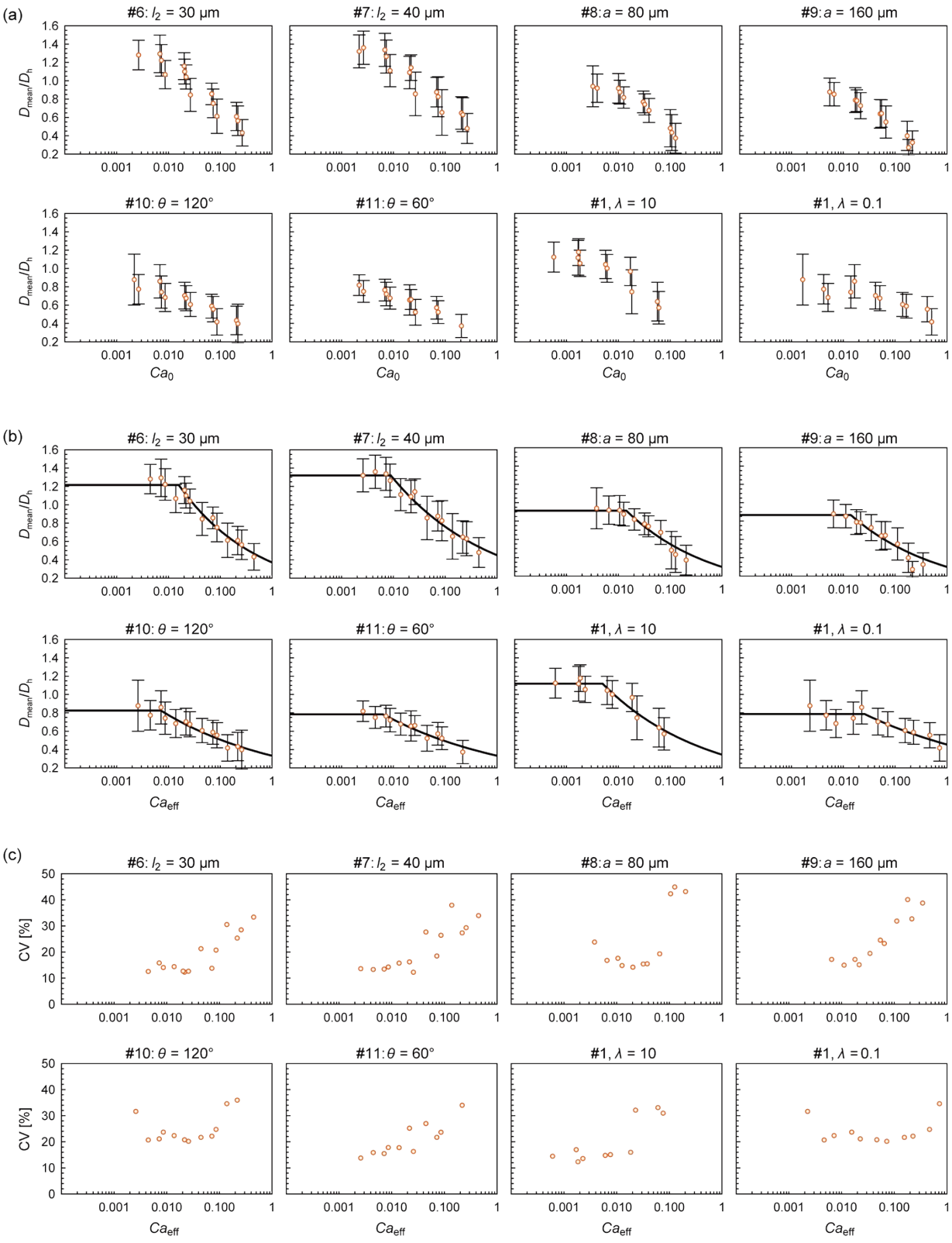

Figure S5 - Variation of normalized droplet diameter D_{mean}/D_h with (a) Ca_0 and (b)Ca_{eff}. Open circles represent experimental data for φ = 0.01–0.33, and solid lines represent fitting curves using Eq. (2). (c) Variation of droplet diameter CV with Ca_{eff}.

Analysis of the droplet fraction in the post-array device

To investigate the effect of non-uniform droplet population (Fig. 2b and c) on D_{mean} in the device, the spatial distributions of droplet velocity, fraction, and diameter at the exit of the post array were measured as shown in Fig. S6 using Image J software. The *xy*-coordinates were set with the origin at the end of the post array, and the velocity distribution was calculated by the particle image velocimetry (PIV) method. The variation of the velocity along the *x*-axis v_x near the post-array ($x = 0$) is shown in Fig. S6b. Fig. S6c and d show the population and the mean droplet diameter measured in the range of $x = 0$–0.4 mm and y = 0–2 mm (area enclosed by a dotted line in Fig. S6a). We found that the flow velocity v_x (Fig. S6b) was inversely proportional to the droplet fraction (Fig. S6c) presumably because the locally increased droplet fraction could lead to a local increase in the effective viscosity and flow resistance. As shown in Fig. 5d, the variation of the mean droplet diameter along the *y*-direction was almost negligible compared to droplet fraction and velocity. As a result, the shear stress, expressed as the product of viscosity and flow velocity, can be almost constant because the increased effective viscosity and the flow velocity cancel out. Thus, we consider that the effective shear stress can be estimated by calculating the emulsion viscosity η_e with the dispersed phase fraction φ.

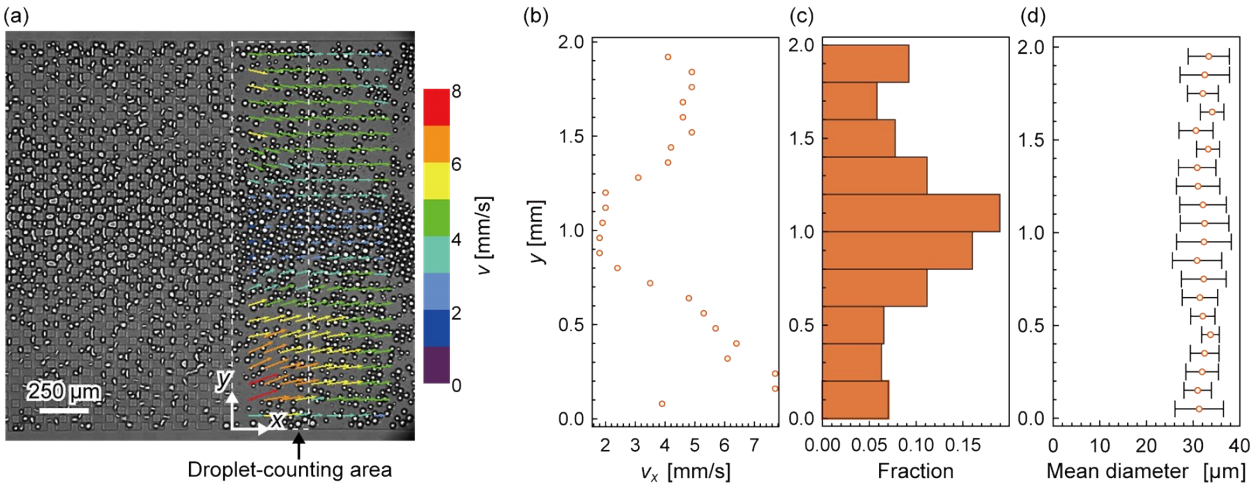

Figure S6 - (a)The flow velocity distribution at the end of post-array obtained by the PIV method with Ca_{eff} =0.018, φ = 0.2, and λ = 1.0 using device #1 and the data in Fig. 2b. A dotted line enclosed area indicates droplet counting area near the exit of the post array. (b) Variation of flow velocity v_x along *x*-direction at the end of the post-array ($x = 0$). Droplet (c) fraction and (d) size distribution within the area of *x* and *y* = 0–0.4 mm and 0–2 mm along the *y*-axis.

Analysis of the bimodal droplet size distribution

We performed an analysis to confirm the cause of the sharp sub-mode seen at D_{mean} = 5–15 μm with Ca_{eff} > 0.05 shown in Fig. 5b. Two normal distributions were fitted to the measured droplet size distributions to quantify the statistical characteristics of the two-modes (Fig. S7a–d). As shown in Fig. S7b–d, the droplet size distributions at Ca_{eff} = 0.002, 0.018, and 0.12 were well-fitted by the sum of two normal distributions. The comparison of the mean droplet diameter of the main and sub-modes and the measured satellite droplet diameter (Fig. S7e–g, n = 1) was shown in Fig. S7a. The mean droplet diameter and its standard deviation were found to decrease significantly after Ca_{eff} = 0.05. Furthermore, the satellite droplet size increased with increasing Ca_{eff}, showing consistency with the sub-mode at Ca_{eff} = 0.1. Thus, the sub-mode mentioned in the main text is mainly caused by promoted satellite droplet generation with high shear stress with Ca_{eff} > 0.05. However, since the distribution shown in Fig. S6c is well represented by the sum of two normal distributions, broad and relatively large sub-mode with gentle shear stress of Ca_{eff} <0.05 may be caused by the asymmetric splitting, as shown in Fig. S7f.

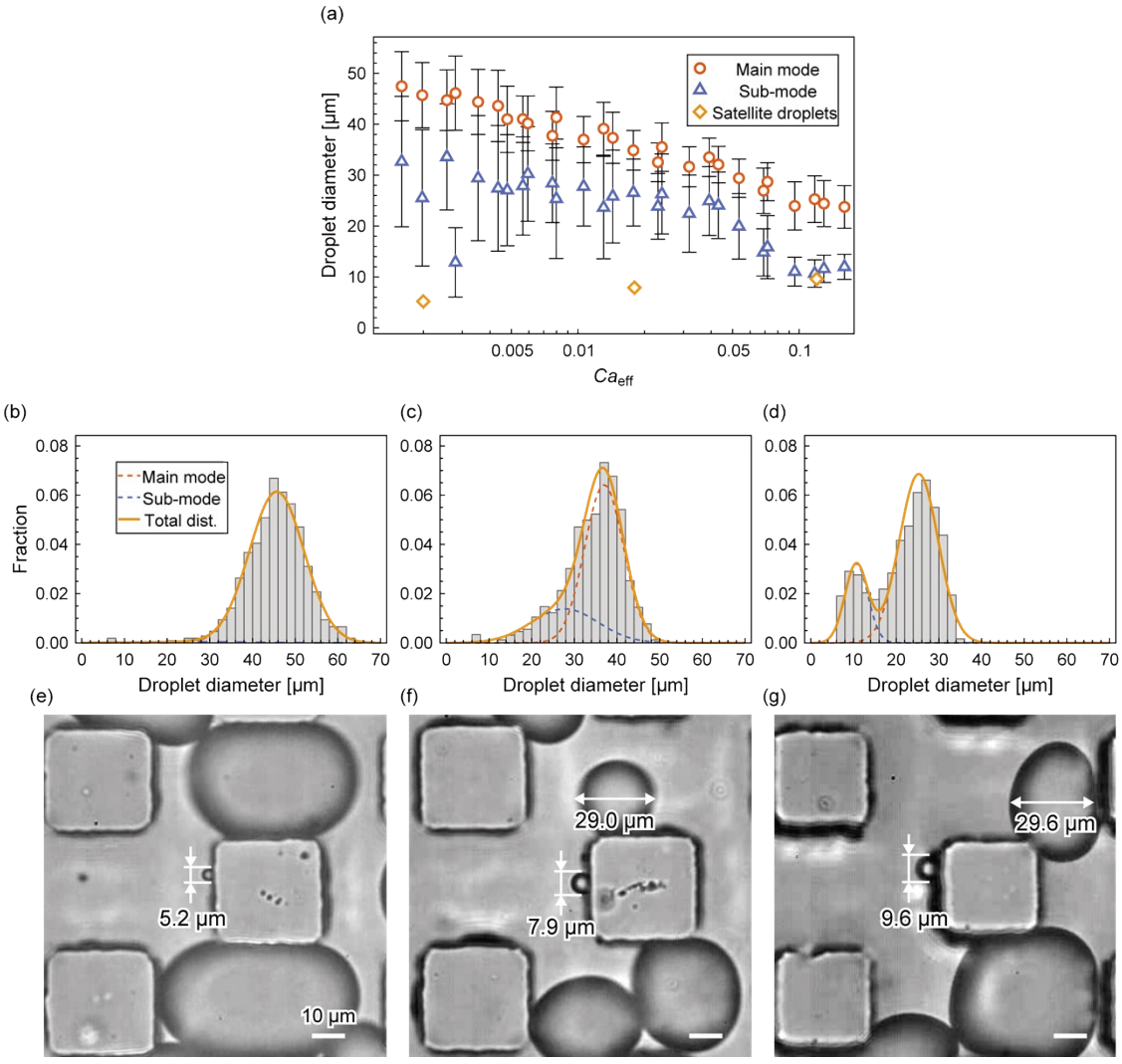

Figure S7 (a)Variation of mean droplet diameter of main and sub-mode obtained by the fitting and the measured diameter of satellite droplets for the same experimental data as Fig. 5b. Fitting results of droplet size distribution by two normal distributions with Ca_{eff} = (b) 0.002, (c) 0.018, and (d) 0.12 and a fixed fraction of = 0.2. Microscopic image of asymmetric breakup and satellite droplet with Ca_{eff}, = (b) 0.002, (c) 0.018, and (d) 0.12 and fixed fraction of φ = 0.2.

Table S1 - Measured viscosity of dispersed and continuous phases.

Material		Viscosity $\eta_{c,d}$ [mPa·s]
PVA	1 wt%	1.6
	8 wt%	17.2
	10 wt%	34.1
Liquid paraffin		16.6
Hexadecane		3.15

Table S2 - Measured interfacial tension of materials.

Condition	Material		Interfacial tension γ [mN/m]	
			Liquid paraffin	Hexadecane
$\lambda = 0.1$	PVA	1 wt%	12.1	-
$\lambda = 1$		8 wt%	10.8	-
$\lambda = 10$		10 wt%	-	11.3

Table S3 - Fitting parameters for each experimental condition.

Conditions		Fitting parameters			
Device index	Label	α	β	Ca_{th}	D_0/D_h
#1	Standard (Data 1)	0.38	−0.19	0.0022	1.20
#1	Standard (Data 2)	0.38	−0.22	0.0060	1.15
#1	Standard (Data 3)	0.39	−0.19	0.0031	1.17
#1	Standard (Data 1-3)	0.39	−0.19	0.0031	1.17
#3	$n_{row} = 100$	0.27	−0.29	0.0052	1.24
#4	$n_{row} = 200$	0.26	−0.30	0.0064	1.19
#5	$n_{row} = 400$	0.31	−0.26	0.0061	1.17
#6	$l_2 = 30$ μm	0.38	−0.28	0.016	1.22
#7	$l_2 = 40$ μm	0.46	−0.22	0.0075	1.34
#8	$a = 80$ μm	0.24	−0.33	0.018	0.91
#9	$a = 160$ μm	0.20	−0.39	0.029	0.83
#10	$\theta = 120°$	0.30	−0.22	0.014	0.79
#11	$\theta = 60°$	0.31	−0.19	0.0092	0.76
#1	$\lambda = 10$	0.25	−0.32	0.010	1.09
#1	$\lambda = 0.1$	0.45	−0.15	0.026	0.79

Movie 1 - Magnified flow image with Ca_0 = 0.0013 and φ = 0.2, recorded at 60 fps. The recording area is 1.2 × 1.2 mm.

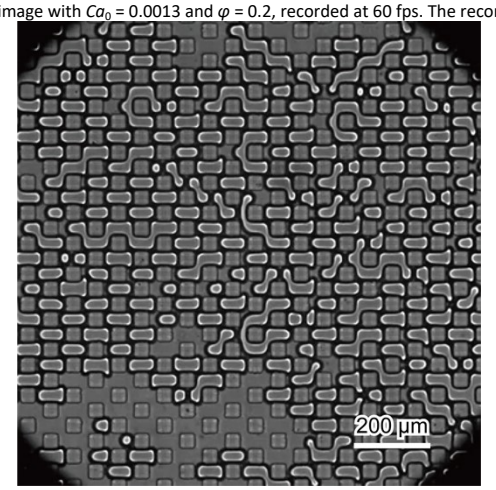

Movie 2 - Magnified flow image with Ca_0 = 0.012 and φ = 0.2, recorded at 250 fps. The recording area is 1.2 × 1.2 mm.

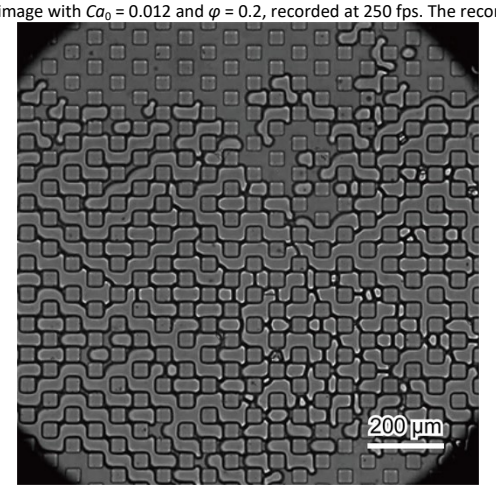

Movie 3 - Magnified flow image with Ca_0 = 0.11 and φ = 0.2 recorded at 2000 fps. The recording area is 1.2 × 1.2 mm.

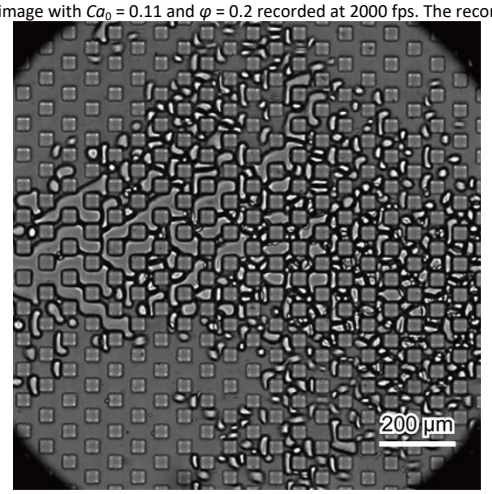

Movie 4 - Flow pattern with different raw capillary numbers Ca_0 and dispersed phase fractions φ recorded at 60 fps.